Materials Research Express

PAPER

Effect of plasma power on reduction of printable graphene oxide thin films on flexible substrates

Indrani Banerjee[1], **Santosh K Mahapatra**[2], **Chandana Pal**[3], **Ashwani K Sharma**[4] **and Asim K Ray**[3]

[1] School of Nano Sciences, Central University of Gujarat, Sector 29, Gandhinagar 382 030, India
[2] Centre of Physical Sciences, Central University of Punjab, Mansa Road, Bathinda 151001, India
[3] Department of Electronic Engineering, Brunel University London, Uxbridge UB83PH, United Kingdom
[4] United States Air Force Research Laboratory, Space Vehicles Directorate, SE Kirtland AFB, NM 87117 United States of America

E-mail: indranibanerjee@bitmesra.ac.in **and** indrani.banerjee@cug.ac.in

Keywords: plasma reduction, graphene quantum dots, density functional theoretical calculation, surface free energy

OPEN ACCESS

RECEIVED
9 January 2018

REVISED
3 April 2018

ACCEPTED FOR PUBLICATION
26 April 2018

PUBLISHED
18 May 2018

Abstract

Room temperature hydrogen plasma treatment on solution processed 300 nm graphene oxide (GO) films on flexible indium tin oxide (ITO) coated polyethylene terephthalate (PET) substrates has been performed by varying the plasma power between 20 W and 60 W at a constant exposure time of 30 min with a view to examining the effect of plasma power on reduction of GO. X-ray powder diffraction (XRD) and Raman spectroscopic studies show that high energy hydrogen species generated in the plasma assist fast exfoliation of the oxygenated functional groups present in the GO samples. Significant decrease in the optical band gap is observed from 4.1 eV for untreated samples to 0.5 eV for 60 W plasma treated samples. The conductivity of the films treated with 60 W plasma power is estimated to be six orders of magnitude greater than untreated GO films and this enhancement of conductivity on plasma reduction has been interpreted in terms of UV-visible absorption spectra and density functional based first principle computational calculations. Plasma reduction of GO/ITO/PET structures can be used for efficiently tuning the electrical and optical properties of reduced graphene oxide (rGO) for flexible electronics applications.

1. Introduction

The first observation in 2004 of ambipolar charge mobility of the order of 1 $m^2V^{-1}s^{-1}$ was made in micromechanically exfoliated; highly ordered, pyrolytic graphite films a few atoms thick at room temperature [1]. Graphene, two-dimensional conjugated sp^2 atoms in a honeycomb structure, has been found in recent years to exhibit unique physical properties such as excellent broad-band optical transparency (≈98%), large thermal conductivity (≈3 kW mK^{-1}) and high mechanical strength ((≈130 GPa). These properties make graphene a promising material for a wide range of applications including field effect transistors [2], photonic devices such as light emitting diodes [3], solar cells [4], hydrogen storage [5], transparent conducting electrodes [6–8], field emitters [9], supercapacitors and batteries [10] and sensors [11]. The graphene oxide (GO) structure is typically a continuous aromatic structure with oxygenated functional groups like epoxides, alcohol, carboxides, ketone carbon lattice interrupted carbonyl etc. This interruption in the lattice array is reflected in the increase of the interlayer spacing of 0.335 nm for graphite to a value ⩾0.625 nm for GO [12]. Therefore, exfoliation of these oxygenated functional groups is necessary to produce a two-dimensional array of graphene. In order to achieve successful low cost commercialisation of these devices, considerable research efforts have been spent on developing fluid dynamic based scalable methods of exfoliation of graphite to produce void–free, high-quality graphene. However, the yield and efficiency of exfoliation remain low [13]. Sonication-assisted reduction of graphite with ascorbic acid is reported to improve the efficiency and yield, producing a few kilograms of graphene per hour [14]. Wafer-size graphene layers have been epitaxially grown on insulating silicon carbide (SiC (0001)) substrates in an argon environment under atmospheric pressure at room temperature. The carrier mobility is found to be higher than the ultrahigh vacuum deposited films by a factor of 2 [15]. The large area

deposition of graphene is possible by chemical vapour deposition on transition metal substrates like Ni, Pd, Ru, Ir and Cu. Cu is found to be a catalyst of superior quality because of its low carbon solubility and catalytic activity towards hydrocarbon gases [16]. The quality of the resulting devices may suffer from unintentional doping and structural damage during the transfer process to electronic-compatible substrates. Thermal lamination and ultraviolet (UV) curable adhesion have recently been employed to address these problems, and when transferred films are doped with gold chloride ($AuCl_3$), the characteristics of the resultant graphene are comparable, as a transparent electrode, to those of indium tin oxide [17]. To overcome these problems, the graphene layer is grown on the interface between the dielectric substrate such as silicon or silicon oxide (SiO_2), silicon carbide (SiC), alumina (Al_2O_3) and the sacrificial catalytic metal via diffusion of methane (CH_4), ethylene (C_2H_4) or solid carbon source through the grain boundaries of metals [18]. Reducing agents like hydrazine (N_2H_4) or sodium borohydride ($NaBH_4$) are used to chemically reduce the GO film and the sheet resistance of $NaBH_4$ reduced GO films is significantly lower than that of a N_2H_4 reduced film. Despite similar C–O compositions in both types of reduced films, simultaneous accumulation of hole-donating nitrogen atoms and removal of oxygen atoms in N_2H_4 reduced films are believed to be responsible for the difference in their electrical behaviour [19]. As many as fifty reducing agents such as hydrohalic acid, L-Cysteines, sulphur- and nitrogen- containing reducing agents, proteins, melatonins and plant extracts have been used, and depending upon the type of reagents used, the conductivity of as–reduced graphene is estimated to range from 12.5 kSm^{-1} to 1.2×10^{-1} Sm^{-1}. The yield of the reduction of graphene oxide with poly (amido amine) dendrimer graphene can be as high as 99% [20]. Some of these reagents are highly toxic, hazardous and not environmentally friendly. Moreover, the chemical reduction processes are not often efficient in achieving complete exfoliation of oxygenated components. Electrochemical methods have now been adopted as a relatively clean physiochemical process using conducting graphite as an electrode (cathode/anode). The intercalation of molecules carrying charges opposite to the electrode takes place producing graphene of relatively high quality with minimal defects and a tunable level of oxidation [21]. Considerable attention has been given in recent years on investigations into wetting transparency of graphene in relation to different types of liquid-substrates interactions. The contact angle of water with completely suspended graphene is found to be 85°, much higher than those with supported graphene. The wetting graphene on the silicon dioxide substrates depend upon largely between short range interaction between graphene and water with only 20% long-range transparency through graphene. The contact angles of water are not significantly influenced by the defects including holes and cracks). The wettability remains largely unaffected by the composition of supporting materials such as air, water, silicon dioxide [22].

Low temperature, green methods of reduction processes such as plasma reduction are efficient for large scale production of highly conducting graphene for flexible electronic applications [23]. The energetic. H+ ions in plasma penetrate into the GO sheets and combine with hydroxyl groups, forming water molecules. Prolonged exposure may therefore have a detrimental effect on the electrical characteristics of reduced GO samples. The optical emission at 884.6 nm may be taken as an indicator of a reduction process [24]. The plasma produced by diffuse coplanar surface barrier discharge in a hydrogen environment has recently been reported to decrease the reduction time without thermal treatment [25]. The removal of oxygen functional groups is found to have enhanced the electrical properties of reduced graphene oxide (rGO). Nearly six orders of magnitude increase of conductivity is reported for Langmuir–Blodgett monolayers of modified Hummers method synthesised GO on Si substrates as the operating temperature of the plasma treatment at 15 W for 30 s is raised from room temperature of 290 K to 223 K [26]. The reduction of GO using H_2/Ar plasma in three different ratios (1:1), (2:1) and (1:2) of varying power between 20 and 100 W indicates that the structure and composition of rGO is determined by the ratio of H_2/Ar, plasma power and treatment time [27]. The exfoliation of oxygenated functional groups from 200 nm thick spin coated graphene oxide (GO) films on a silicon substrate has recently been achieved by 60 W hydrogen plasma treatment. The removal of oxygen functional groups is found to have enhanced the electrical properties of reduced graphene oxide (rGO). The sheet resistivity determined from Van der Pauw measurements was 1.62 MΩ/square, yielding a value of −3.1 Sm for the bulk conductivity. The electron mobility of 37.53 $cm^2V^{-1}s^{-1}$ is determined for reduced GO film by the Hall measurement technique [28]. In the present investigation, commercially available graphene oxide (GO) nanoparticles have been utilised to produce solution processed thin films of GO on indium tin oxide (ITO) coated polyethylene terephthalate (PET) substrates and these films have then been reduced by a 30 min duration treatment with RF hydrogen plasma of powers varying between 20 W and 60 W at room temperature in the ordinary laboratory environment. X-Ray diffraction patterns and Raman spectra have been studied for evaluation of structural changes due to plasma treatment. UV-visible absorption spectra have been recorded. The conductivity of GO films is estimated from the current-voltage characteristics recorded in room temperature under vacuum for sandwich configurations of the samples between the substrates and platinum top electrodes. The band gap has been estimated from the density functional based first principle computational calculations. The surface free energy (SFE) have been determined from the contact angle measurements of water on GO and go films on the ITO substrates to examine the effect of reduction on the wettability.

2. Experimental details

Using a KW-4A spin coater from the Chemat Technology Inc., USA, 300 nm thick GO films were prepared for electrical measurements by spin-coating a small volume of the spreading solution on cleaned ITO/PET substrates at 850 rpm and 2500 rpm in a sequence for 15 and 60 s, respectively at room temperature. The spreading solution contains the dispersion of commercially available GO sample in water (Sigma Aldrich) by 40% by weight. Prior to the deposition, the substrates had been previously cleaned with acetone and distilled water. After complete removal of the aqueous solvent by heating in an oven at 100 °C, the dry samples were treated with 30 min long RF hydrogen plasma using a Gatan Solarus model 950 plasma cleaner at room temperature under atmospheric pressure. Plasma powers of 20 W, 40 W and 60 W were employed to examine the effect of on GO reduction in terms of structural and morphological, optical, electrical and wetting properties.

2.1. Characterization of GO thin films

The graphene oxide and plasma reduced graphene oxide samples were characterized by means of x-ray diffraction using a Bruker D8 advance scanning instrument. The Cu K_α radiation of wavelength 0.154 06 nm was used with scattering angle varied between 10° and 90° at a scanning rate of 0.02 per sec for the crystallographic analysis of the samples. The UV–vis absorption spectra of the spin coated GO on ITO coated PET substrates were recorded using Perkin-Elmer LAMBDA 650 spectrometer between 400 to 800 nm with the scanning rate of 654.8 nm min^{-1}. The water optical contact angle for the samples was measured with an OCAH 230(Data Physics, Germany). The technique used in this investigation was a sessile drop method with a water drop of volume 2 μl [29]. The average of three readings for the same sample has been recorded with an accuracy of measurement of ±1°. The Fourier transform infrared spectroscopic (FTIR) spectra were acquired in the range of 500–4000 cm^{-1} using Shimadzu Corp., Japan, and Model IR-Prestige 21. The data acquisition was performed in transmission geometry. The microstructure of the samples was observed by Scanning Electron Microscopy (SEM) JEOL Model No. SEM3400N. The Raman spectrum was obtained using a Horiba Jobin Yvon Lab RAM HR800 with incident laser beam of wavelength 514.5 nm with 2 μm spot size. Using a Keithley 617 electrometer in a microprocessor controlled system, the current (I) passing through the graphene samples sandwiched between PET coated ITO substrate and sputtered platinum (Pl) as the top electrode was measured under vacuum of 10^{-5} mbar as the bias voltage (V) was swept from +1 V to −1 V through 0 V at the scan rate of 500 mV s^{-1} with respect to the grounded bottom PEL/ITO electrode. $A = 0.5$ cm^2 is the effective diode area and the film thickness t is 300 nm thick.

2.2. Computation of lattice and electronic structure

The first principle density functional theoretical (DFT) study was made on GO and rGO samples by using the SIESTA (*Spanish Initiative for Electronic Simulations with Thousands of Atoms*) software package which employs norm-conserving pseudo-potential [27]. The visualization software GDIS MOLECULE MODELLER was used to simulate the structure of GO [30]. The distance between the periodic images of the graphene oxide layer was kept at more than 1 nm to avoid mutual interaction. In addition, calculations were performed by choosing the reciprocal space which is sampled by a grid of 20 × 20 × 1 points and generalised gradient approximation (GGA) exchange correlation functions. Fully relax coordinates are used where the force on each atom is less than 0.4 $eVnm^{-1}$.

3. Results and discussions

The SEM images in figure 1 show the wrinkled morphology of the surfaces of both as-deposited and plasma treated GO samples. However, the density of wrinkles becomes greater on plasma treatment (figures 1(a) and (b)). The structure of a single wrinkle is presented in figures 1(c) and (d) under the same resolution. It is interesting to observe that the width of the wrinkle is reduced from 2.15 μm to 300 nm on plasma treatment. This type of wrinkled surface morphology agrees with one observed for the chemically reduced GO, indicating the overlapping of the flakes in go [31].

The X Ray diffractogram in figure 2(i) show the two peaks at $2\theta \sim 10°$ and $2\theta \sim 26.15°$ associated with the diffraction at the (001) and (002) planes, of graphene oxide and that of reduced graphene oxide after plasma treatment respectively. These peak positions agree well with those observed for the structure of a UV reduced GO sample on the PET substrate, originally synthesised by the modified Hummers method [32]. The spectra show significant rise in the peak intensity from (002) planes with increasing plasma power as shown in figure 2(b) with subsequent decrease in the reflection intensity from (001) plane of graphene oxide sample (untreated sample). This indicates that plasma irradiation significantly reduces the oxygenated functional

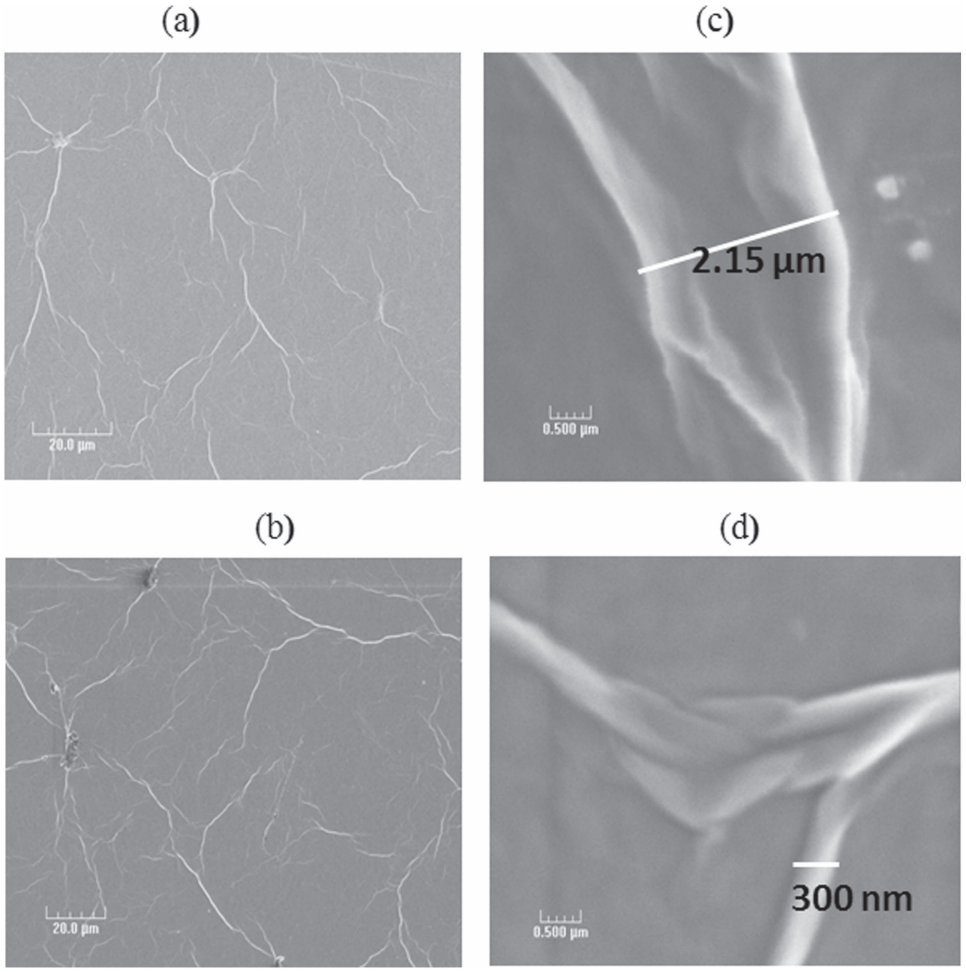

Figure 1. SEM micrographs for (a) as-deposited and (b) 60 W plasma treated GO samples. A single wrinkle in (c) as-deposited and (d) 60 W plasma treated GO samples.

groups from the graphene oxide samples. Values of the interlayer spacing distances are estimated from the Bragg law and the significant decrease in values from 0.88 nm for as-prepared graphene oxide to 0.35 nm for reduced graphene oxide. The interlayer distance of 0.35 nm for the graphitic planes is found to be close to the van der Waals thickness of atomically flat graphene [33]. Using the Debye–Scherrer formula in the form of $\boldsymbol{L} = \frac{K\lambda}{\beta \cos \theta}$ [34] the average crystallite size L was estimated from the full width β at half maximum (FWHM) of (002) peak and it is found that the crystallite size almost remains the same at 5.7 nm irrespective of the plasma power. The number N_{GL} of layers has been estimated to be 15 from the expression $L = (N_{GL} - 1)\, d_{002}$ where, d_{002} represents the thickness as measured from the centre of the sample. The stacking of these layers is believed to be responsible for the intensity and sharpness of the [002] peak. The observations show significant reduction of the graphene oxide through removal of oxygenated functional groups from the graphene oxide [35]. Figure 2(ii) gives the plot showing the variation of ratio of intensity I_{RGO} to I_{GO} (open triangles) corresponding to the (002) plane X Ray reflection and average crystal size L (open circles) with plasma power.

The FTIR spectra in figure 3 show the chemical changes involving functional groups because of the plasma reduction of GO. The presence of oxygenated functional groups such as C–O–C at 1011 cm^{-1}, C–OH at 1200 cm^{-1}, O–H bending at 1680 cm^{-1}, and –OH stretching between 3400–400 cm^{-1} was observed for all samples. The peak positions agree with the values reported for tri-layered graphene oxide reduced by N_2 and O_2 plasma [36]. The antisymmetric vibrations for graphitic CH_2 are also present at 2816 cm^{-1}. The peak at 1570 cm^{-1} may be identified with the skeletal vibration of the graphitic domain [37]. The intensity for the 60 W plasma reduced sample shows significant decrease in intensity for the oxygenated functional groups of C–O–C and C–O–H.

Figure 4(a) shows the Raman spectra of the samples, identifying the structural changes occurring due to plasma treatment. The characteristic D and G_{app} band appears at ~1350 cm^{-1} and ~1578 cm^{-1}. The D band

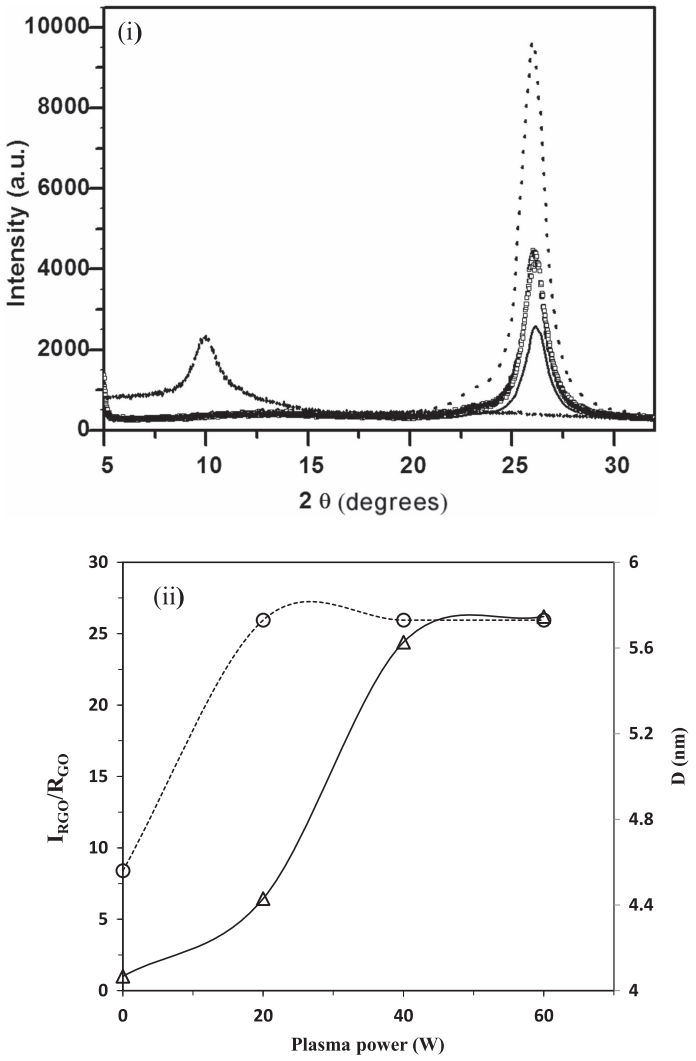

Figure 2. (i) XRD spectra for dashed line for GO, solid line for 20 W, squared line for 40 W and dotted line for 60 W plasma treated samples (ii) variation of ratio of intensity I_{RGO} to I_{GO} (open triangles) corresponding to the (002) plane X Ray reflection and average crystal size D (open circles) with plasma power.

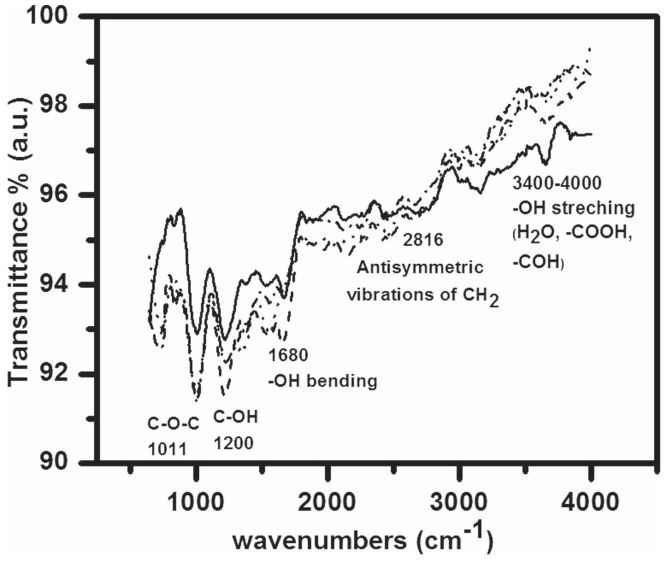

Figure 3. FTIR spectrum from 4000 cm^{-1} to 500 cm^{-1} for samples: untreated (dotted line) and plasma treated with 20 W (broken line with dots), 40 W (broken line) and 60 W (solid line).

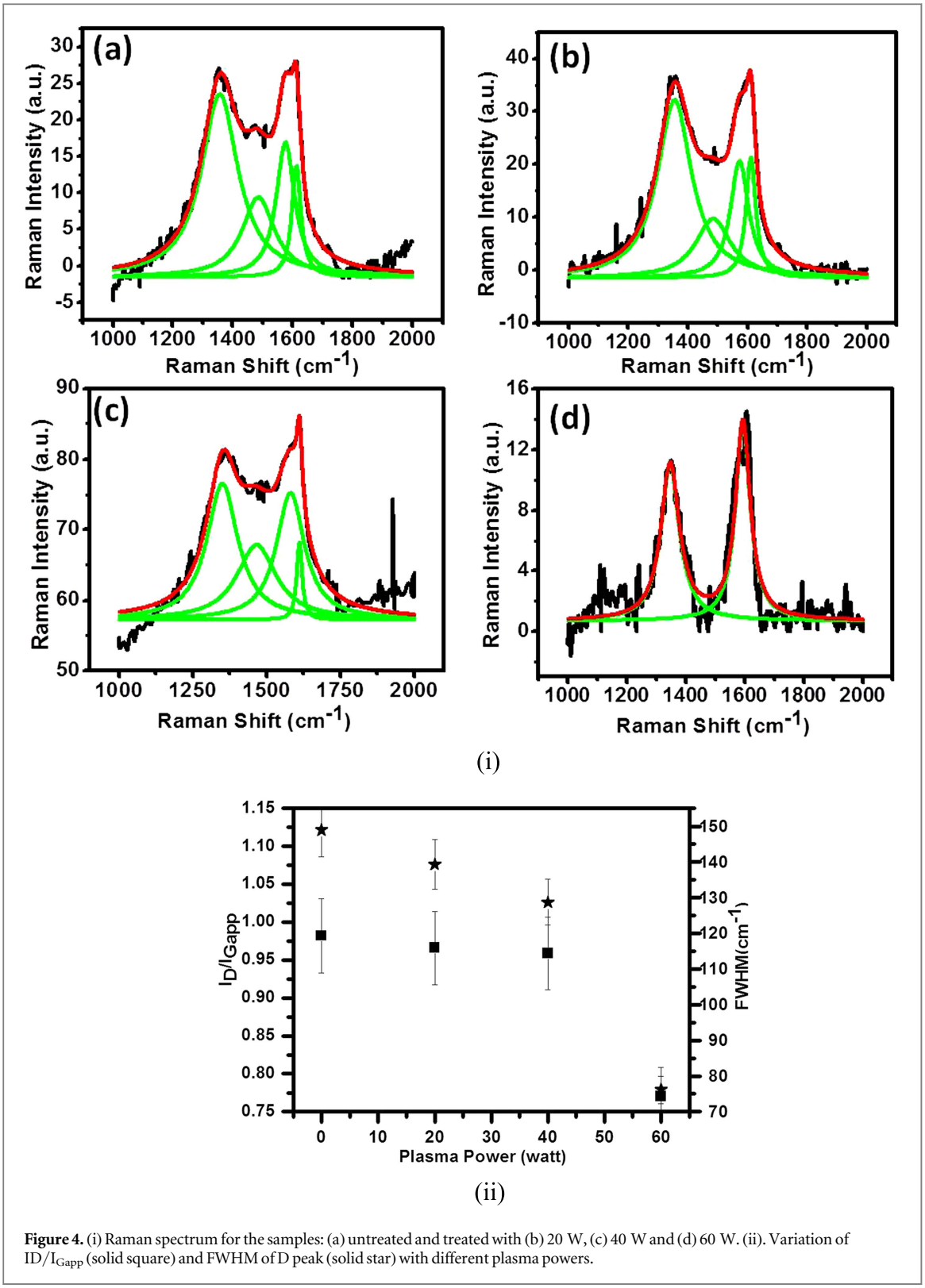

Figure 4. (i) Raman spectrum for the samples: (a) untreated and treated with (b) 20 W, (c) 40 W and (d) 60 W. (ii). Variation of ID/I_{Gapp} (solid square) and FWHM of D peak (solid star) with different plasma powers.

response originates due to defects or translational disorders whereas the G_{app} band corresponds to scattering from the E_{2g} mode of the sp^2 graphitic domain superposed with contributions from D′, D + D′, and 2D′ [38–40]. The presence of a broad shoulder peak has been observed between D and G_{app} band for the untreated, 20 W and 40 W plasma treated samples which disappears for the 60 W plasma treated sample. The significant disappearance of the shoulder peak between D and G_{app} band confirms the reduction process of GO through plasma treatment [41]. The Raman spectra also shows that due to plasma treatment the D and G_{app} bands are shifted from 1348.3 cm^{-1} to 1357.7 cm^{-1} and from 1594.7 cm^{-1} to 1593.5 cm^{-1} respectively along with

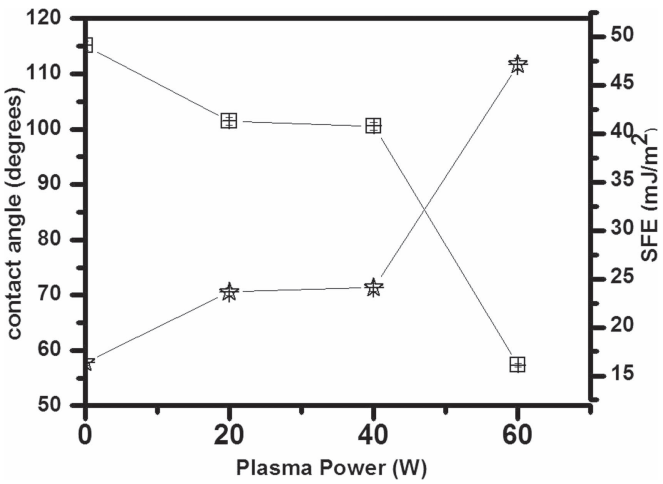

Figure 5. Variation of contact angle (squares) of the samples for water and surface free energy (stars) with Plasma power.

decrease in the full width half maximum of the disordered D peak. Figure 4(b). shows the variation of intensity ratio of (I_D/I_{Gapp}) and FWHM of D peak with respect to the plasma powers. In order to obtain a quantitative idea of the effect of plasma treatment on the structural morphology of the sample, a Lorentzian method of curve fitting has been performed. The intensity ratio of the D and G_{app} bands (I_D/I_{Gapp}) has significant effect in determining in-plane sp^2 crystallite size (L_a) which may be taken to be the inverse of this ratio according to the model of Tuinstra-Koenig [42] given as given as $L_a = \frac{560}{E^4}\left(\frac{I_D}{I_G}\right)^{-1}$ where, E represents the energy (2.41 eV) of the incident laser source used for the present work. The decrease in (I_D/I_{Gapp}) ratio signifies corresponding increase of the in-plane sp^2 graphitic domain size from 16.9 nm, 17.1 nm, 17.3 nm to 21.55 nm for untreated, 20 W, 40 W and 60 W plasma power treated samples respectively. A similar decrease in the intensity ratio has been reported for the reduction of graphene oxide by hydrazine hydrate which corresponds to the decrease in sp^2 cluster size on account of defects, oxygen vacancies or distortions induced in the sp^2 domains due to oxygen extraction [43]. The defect limit (L_D) given as $\frac{I_D}{I_G} = \frac{A}{L_D^2}$, where the value of A $\sim$ 100 nm^2 for the incident laser wavelength of 514 nm could be estimated for the samples with gradual exposure of the plasma power [38, 39]. The relation is valid for larger values of L_D ($L_D > 6$ nm) and for $L_a > L_D$. The defect limit for the present samples varied from 10.09, 10.17, 10.21 and 11.39 for untreated, 20 W, 40 W and 60 W plasma powers respectively. The increase in defect limit signifies multiple stages of reduction from highly defective stage II to less defective stage I transition happening due to plasma treatment. It may be inferred that plasma treatment has induced conversion of high defective graphene oxide to less defective reduced graphene oxide samples.

Figure 5 shows the optical contact angle θ of untreated and hydrogen plasma treated GO samples on indium tin oxide (ITO) substrates with water. The contact angle significantly increases from 57.84° for an untreated GO sample to 111.71° for GO treated with hydrogen plasma of 60 W. This shows that the film changes from hydrophilic to hydrophobic due to the exfoliation of oxygenated functional groups with increase of hydrogen plasma power, making the reduced graphene more difficult to wet than graphene oxide. The contact angles for graphene depend upon the number of layers and the substrate, for example, values of 90.6° and 158° have been reported for 6–9 layers of graphene on copper and Si substrates, respectively [44]. The water-graphene-solid effective interaction potential per unit area W_A is usually determined from the contact angle θ using the Young Dupre equation in the form [45]:

$$W_A = \gamma_l(1 + \cos\theta) \tag{1}$$

where, γ_l is the interfacial surface tension between liquid and the vapour, which is equal to 72.8 mg m^{-2} for water, and θ is the contact angle. The surface free energy (SFE) γ_s of the samples was determined using the equation of state approach by the given relation [46]:

$$\cos\theta = -1 + 2\sqrt{\frac{\gamma_s}{\gamma_l}}e^{-\beta(\sigma_l-\sigma_s)^2} \tag{2}$$

β is an empirical constant equal to 1.247 $\times$ 10^{-4} $(m^2/mJ)^2$. The SFE for the samples was computed using Newton's iterative method. The reduction of oxygenated functional entities from the sample surface considerably decreases the surface energy. The hydrophilic surfaces of graphene oxide flakes on silicon substrates become hydrophobic on chemical exfoliation by hydrazine. Values of contact angles with water, surface adhesion and SFE are found to be in satisfactory agreement with those obtained in the present investigation [47].

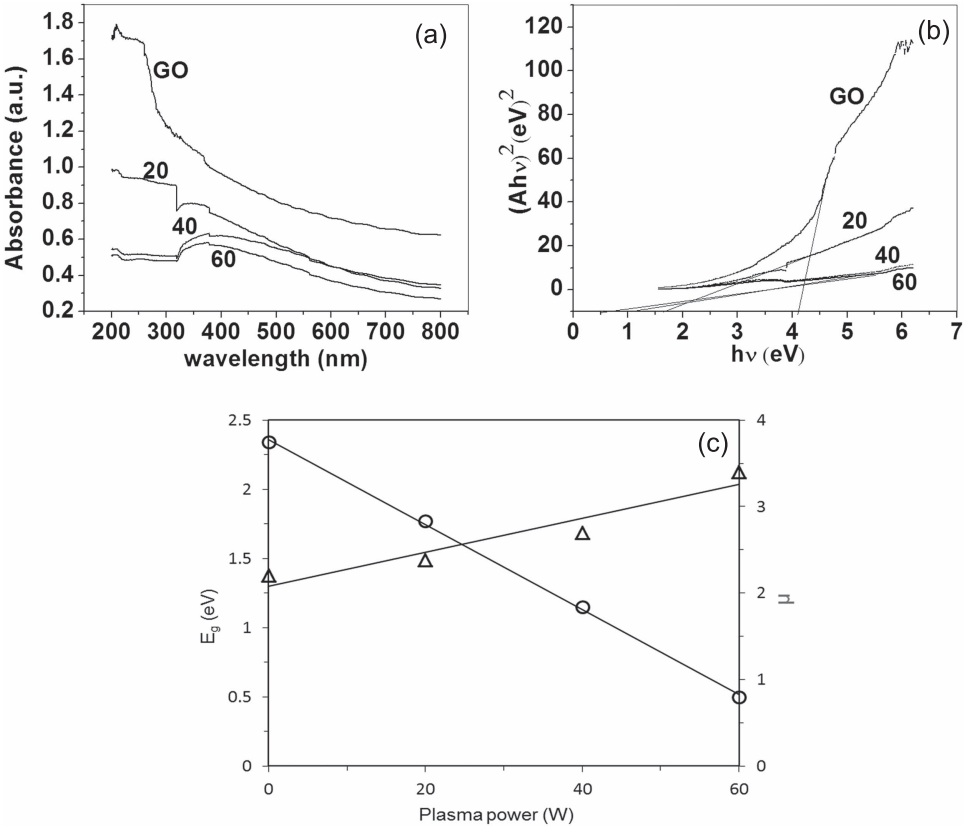

Figure 6. (a) UV–vis spectra (b). Tauc plot obtained from UV–vis spectra for untreated and plasma treated samples. (c) Dependence of optical bandgap E_g (circles) and refractive index μ (triangles) on plasma power.

UV spectra are presented in figure 6(a) showing absorbance A as a function of incident photon energy hν. The maximum absorption between 200 nm and 300 nm is attributed to (i) π-π^* transition from the conjugated C–C bonds present in the original graphitic structure and (ii) π-π^* transition from the unsaturated carboxylic groups such as ketones, carboxylic acids [48]. The observation of a shoulder peak in the spectrum for 60 W plasma treated films at around 300 nm may be attributed to the π-π^* transition from the carbonyl groups. A red shift in the λ_{max} indicates the reduction process in the graphene oxide samples after plasma exposure [49]. The optical band gap E_g is estimated from the intercept on the abscissa ($h\nu$) of Tauc plots for $(A(h\nu))^2 = 0$ in figure 6(b) as given by the equation for the indirect interband transition in the form [50]:

$$A(h\nu) = A_0 \exp\left(\frac{\sigma(h\nu - E_0)}{k_B T}\right)^{0.5} \tag{3}$$

As shown in 6(c), values of the band gap decrease from 4.1 eV to 0.5 eV with the increase of plasma power from 30 W to 60 W. This behaviour is consistent with the results obtained for reduction of GO upon a week-long exposure to hydrazine vapours at room temperature. The decrease of E_g to 0.5 eV may, therefore, be identified with the removal of organic moieties such as carbonyl and tertiary alcohol groups [51]. The exfoliation of the oxygenated functional groups due to plasma treatment is also expected to affect the refractive index of the samples. Values of the linear refractive index μ for the samples were calculated from the Lorentz-Lorentz equation for electronic polarizability as [52],

$$\frac{\mu^2 - 1}{\mu^2 + 1} = 1 - \sqrt{\frac{E_g}{20}} \tag{4}$$

The refractive index for the untreated sample was determined to be 2.2, whereas after plasma treatment the refractive index increases to 3.4 for 60 W plasma exposures. These values are in good agreement with pico-metrology measured values for graphene monolayer on silicon grown with SiO_2 substrates [53].

The optimised structures of GO samples with 100%, 75%, 25% and 0% of residual O atoms using SIESTA computational programme are shown in figure 7. As shown in the top view of figure 7(a), the formation of epoxy functional groups been each of oxygen atoms in a fully oxidized sample (with 100% residual O atoms) with two neighboring C atoms on the opposite sides the graphene lattice is believed to be responsible for the Coulomb

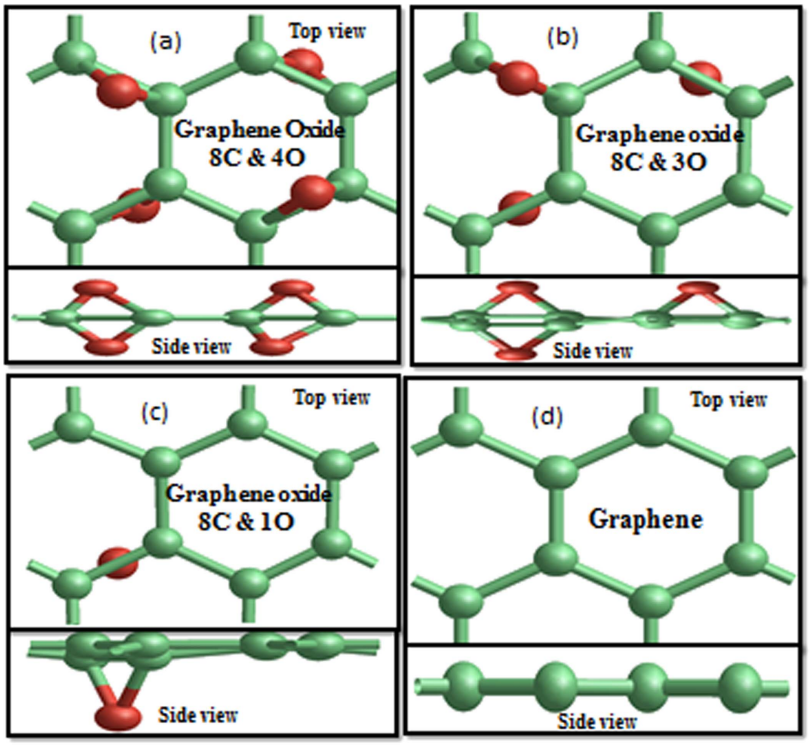

Figure 7. Top and side views of atomic structure of (a) GO with 100% oxygen (b) rGO with 75% oxygen (c) rGO with 25% oxygen and (d) Graphene with 0% oxygen. Red colour spheres represents for Oxygen atom and green spheres represent for Carbon atom.

repulsion energy minimisations. As a result, the C atoms are vertically displaced from 2D hexagonal lattice structures due to the strain caused by sp^3 hybridisation between C and $2p_z$ orbitals as shown in the side view of figure 7(a). The GO samples are optimised by selective removal of oxygen (O) atoms from its pristine GO structure. It is observed from figures 7(b), (c) and (d) that buckling structure is converted to in- plane structure with reduction of oxygen from 100% to 0%. The band diagrams $E(k)$ of the samples with 100%, 75%, 25% and 0% of residual O atoms using SIESTA computational programme are shown in figure 8. As it can be seen figure 9, values of the simulated band gap E_g rise monotonically from $E_g = 0$ eV to $E_g = 4.27$ eV with the increase in oxygen vacancy corresponding to 0% and 100% residual oxygen atoms, respectively. Similar the decrease of E_g on reduction is estimated from the reported *ab initio* and hybrid density functional theory (DFT) calculations [54]. The reduced GO may be considered as a 2D structure containing randomly distributed graphene quantum dots (GQDs) across the GO surface, forming graphene islands of different sizes [55]. Values of the binding energy E_b of C atoms at the boundaries of GQDs to GO layer is seen from figure 9 to be decreasing from −12.26 eV to −9.48 eV as percentage of residual oxygen decreased from 100% to 0%, indicating the degree of stability of samples.

The GQDs play an important role of the carrier transport in reduced GO samples as shown in figure 10 shown in the reproducible I (V) curves of the samples for the bias voltage V cycles between ±1 V. The conductivity σ of the 60 W plasma rGO is found to increase over that of the untreated GO sample by a factor of 10^6. This enhancement of conductivity is significantly encouraging in comparison to the reported rise in conductivity by less than one order magnitude for wrinkled go films chemically reduced by hydrazine at 80 °C [56]. As the decrease in the bandgap occurs with the decline in the oxygen to carbon ratio and this factor is believed to be responsible for the enhancement in conductivity in the reduced GO samples. The energy barrier height at the metal and dielectric interface may be lowered by the image force and the mechanism may be characterised by (i) asymmetric factor (η), (ii) field lowering coefficient β_s and (ii) the barrier height φ_b between the Fermi-level of the injecting Pt electrode and the conduction band minimum of GO films, The asymmetry factor η is defined as the ratio of $\frac{I_-}{I_+}$ where I_+ and I_- correspond to the values of current at the negative and positive biases, respectively. The current I is limited by Schottky emission over the barrier height φ_b in the form [57]:

$$I = AA^*T^2\left(\exp\left(-\frac{q\varphi_b - \beta_s V^{1/2}}{k_B T}\right)\right). \quad (5)$$

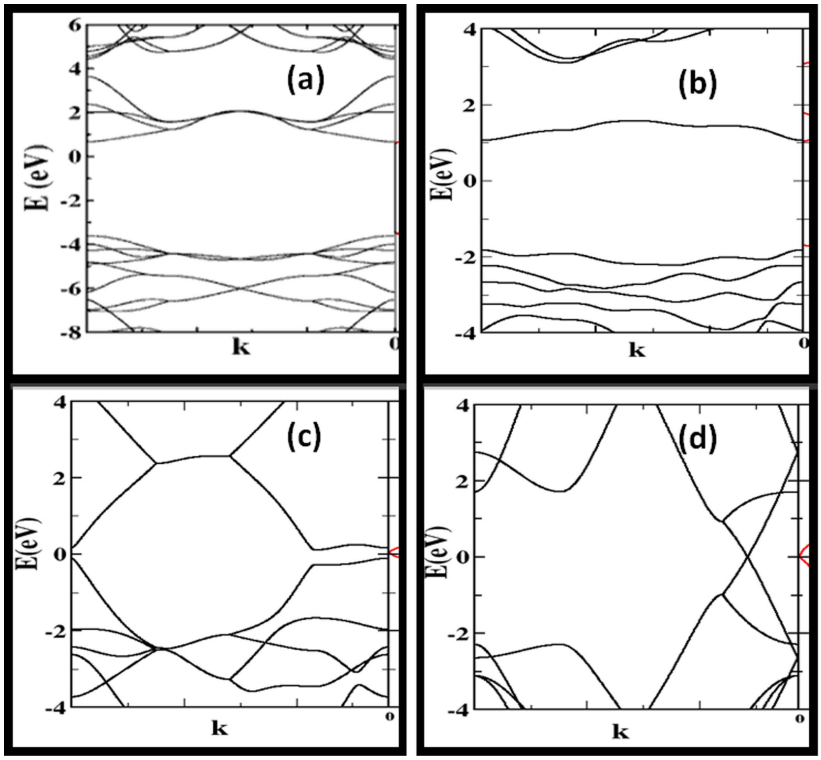

Figure 8. Band structure of (a) GO with 100% oxygen (b) rGO with 75% oxygen (c) rGO with 25% oxygen and (d) Graphene with 0% oxygen. (e) Plot of binding energy E_b and band gap E_g with respect to residual oxygen in %.

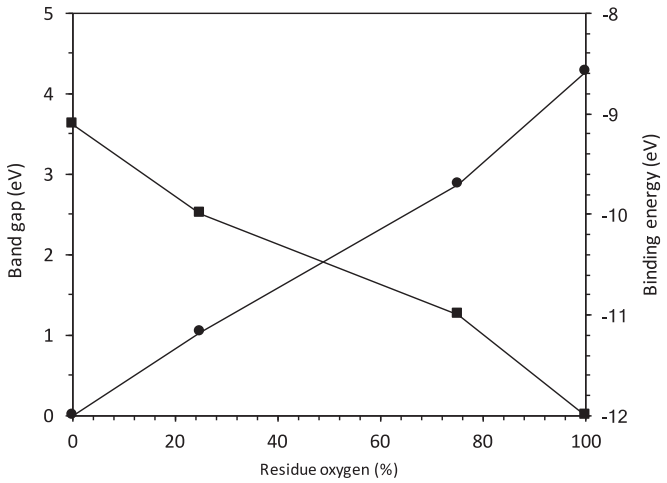

Figure 9. Plot of binding energy E_b (circle) and band gap E_g (square) with respect to residual oxygen in %.

where $A = 0.5\ \text{cm}^2$ is the effective diode area *and* the effective Richardson constant $A^* = \frac{120m^*}{m_0}$ where m^* and m_0 are the effective electron mass in the dielectric films and free electron mass, respectively and $q = 1.6 \times 10^{-19}$ C is the electronic charge. For GO films, a value of 0.44 is taken to be the ratio of $\frac{m^*}{m_0}$ [58]. Values of φ_b and β_s are estimated by numerically fitting equation (5) to experimental data and the results are summarised in table 1. Values of η are found to be nearly equal to be unity for all reduced GO samples. This implies that the conduction is primarily a bulk limited process involving the density and size of GQDs. The significant decrease in φ_b from 0.58 eV for untreated GO films to 0.26 eV for 60 W power treated films with is consistent with the earlier observation on optical band gap values, indicating the improved alignment between the Fermi level of the platinum electrode and conduction band edge of the graphene oxide samples. Also, reduction dependent increase in values of β_s is also a contributing factor for enhanced charge flow.

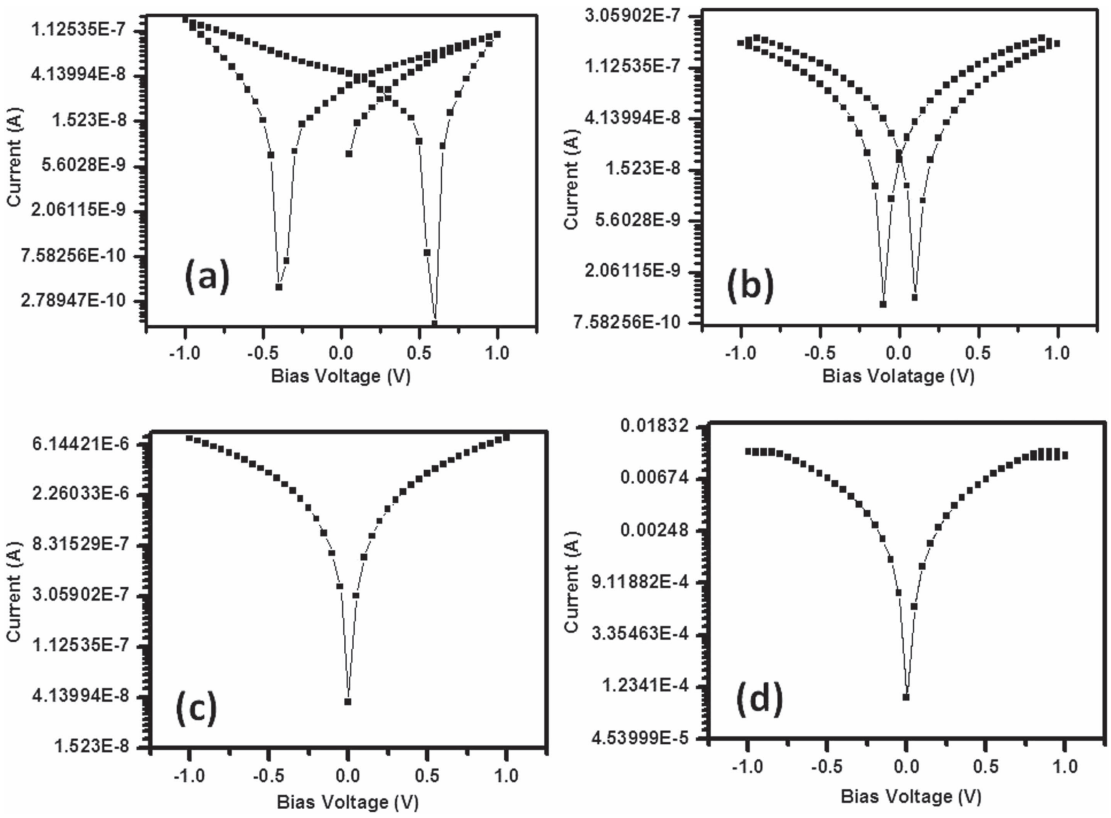

Figure 10. I (V) characteristics of the samples: (a) untreated and treated with the plasma power of (b) 20 W, (c) 40 W and (d) 60 W.

Table 1. Parameters obtained from I(V) characteristics of the samples from equation (5).

Plasma power (W)	η (I_-/I_+)	φ_b (eV)	β_s
0	1.3	0.58	2.8×10^{-10}
20	1.01	0.55	1.3×10^{-9}
40	0.9	0.47	2.1×10^{-8}
60	0.991	0.26	5.03×10^{-6}

4. Concluding remarks

Room temperature hydrogen plasma-assisted reduction of graphene oxide films on flexible substrates has been studied. The wrinkled surface structures have been observed in SEM images with the density of wrinkles in rGO higher than GO films. The fast exfoliation of the oxygenated components has been studied using XRD and **Raman spectroscopy** leading to the formation of sp^2 graphitic domains. The computational values of energy bandgap are consistent with those estimated from optical absorption spectra, showing the rise of energy gap with the increase in oxygen vacancies. Plasma treatment has proved to be an efficient, low temperature, fast method of reduction of graphene oxide on flexible substrates with significantly significant improvement in conductivity. The hydrophilic surfaces of GO become hydrophobic on plasma reduction making the reduced graphene more difficult to wet than graphene oxide. The direct reaction of non-equilibrium low temperature plasma generating energetic hydrogen with the sp^3 or the oxygenated functional group rather than with the sp^2 group may be responsible for this behaviour. It should also be pointed out here that conduction is also consistent with our computation results of bandgap. The use of commercially available GO sample offers tremendous opportunities for low cost fabrication of new generation devices over large area flexible substrates.

Acknowledgments

Dr Indrani Banerjee is grateful to Commonwealth Association, UK for funding the present research work under the fellowship placement scheme (Grant reference INCF-2014-66). The subsequent visit of Dr Banerjee is partially

sponsored by the Air Force Office of Scientific Research, Air Force Material Command, USAF, under Grant No. FA9550-15-1-0123. Gratitude is due to Dr Lesley Hanna of the Institute of Materials and Manufacturing, Brunel University London for help in preparing the manuscript.

ORCID iDs

Asim K Ray https://orcid.org/0000-0002-5392-0041

References

[1] Novoselov K S, Geim A K, Morozov S V, Zhang D, Zhang Y, Dubonos S V, Grigorieva I V and Firsov A A 2004 *Science* **306** 666–9
[2] Han T H, Kim H, Kwon S J and Lee T W 2017 *Mater. Sci. Eng. R-Rep.* **118** 1–43
[3] Choi S H 2017 *J. Phys. D-Appl. Phys.* **50** 103002
[4] Ubani C A, Ibrahim M A, Teridi M A M, Sopian K, Ali J and Chaudhary K T 2016 *Sol. Energy* **137** 531–50
[5] Szczesniak B, Choma J and Jaroniec M 2017 *Adv. Colloid Interface Sci.* **243** 46–59
[6] Bointon T H, Russo S and Craciun M F 2015 *IET Circ. Devices Syst.* **9** Special Issue: SI 403–12
[7] Kumar P, Singh A K, Hussain S, Hui K N, Hui K S, Eom J, Jung J and Singh J 2013 *Reviews in Advanced Sciences and Engineering* **2** 1–21
[8] Hussain S, Iqbal M W, Park J, Ahmed M, Singh J, Eom J and Jung J 2014 *Nano Scale Research Letters* **9** 546
[9] Chen L F, Yu H, Zhong J S, Song L H, Wu J and Su W T 2017 *Mater. Sci. Eng. B-Adv. Funct. Solid-State Mater.* **220** 44–58
[10] Eng A Y S, Sofer Z, Simek P, Kosina J and Pumera M 2013 *Chem.-Eur. J.* **19** 15583–92
[11] Justino C I L, Comes A R, Freitas A C, Duarte A C and Rocha-Santos T A P 2017 *Trac-Trends Anal. Chem.* **91** 53–66
[12] He H Y, Klinowski J, Forster M and Lerf A 1998 *Chem. Phys. Lett.* **287** 53–6
[13] Yi M and Shen Z G 2015 *J. Mater. Chem.* A **3** 11700–15
[14] Abdolhosseinzadeh S, Asgharzadeh H and Kim H S 2015 *Sci. Rep.* **5** 10160
[15] Emtsev K V *et al* 2009 *Nat. Mater.* **8** 203–7
[16] Mattevi C, Kim H and Chhowalla M 2011 *J. Mater. Chem.* **21** 3324–34
[17] Kang M H, Milne W I and Cole M T 2015 *IET Circ. Devices Syst.* **9** 39–45
[18] Ning J, Wang D, Chai Y, Feng X, Mu M S, Guo L X, Zhang J C and Hao Y 2017 *Nanotechnology* **28** 284001
[19] Shin H J *et al Adv. Funct. Mater.* 2009 **19** 1987–92
[20] Chua C K and Pumera M 2014 *Chem. Soc. Rev.* **43** 291–312
[21] Feng X Y, Chen W F and Yan L F 2016 *RSC Adv.* **6** 80106–13
[22] Ondarcuhu T, Thomas V, Nunez M, Dujardin E, Rahman A, Black C T and Checco A 2016 *Sci. Rep.* **6** 24237
[23] Lee S W, Mattevi C, Chhowalla M and Mohan Sankaran R 2012 *J. Phys. Chem. Lett.* **3** 772–7
[24] Kim M, Kahng Y H, Kim Y J, Kumar T P, Park T K, Lee K and Jang J H 2013 *AIP Adv.* **3** 032121
[25] Bodik M, Zahoranova A, Micusik M, Bugarova N, Spitalsky Z, Omastova M, Majkova E, Jergel M and Siffalovic P 2017 *Nanotechnology* **28** 145601
[26] Singh G, Botcha V D, Sutar V D S, Narayanam P K, Talwar S S, Srinivasa R S and Major S S 2014 *Phys. Chem. Chem. Phys.* **16** 11708–18
[27] Li J, Chen C L, Wei J, Li J X and Wang X K 2014 *J. Phys. Chem.* C **118** 28440–7
[28] Li T Y, Patel T, Banerjee I, Pearce-Hill R, Gallop J, Hao L and Ray A K 2015 *J. Mater. Sci.-Mater. Electron.* **26** 4810–5
[29] Garbassi E, Morra M and Occhiello E 1994 *Polymer Surfaces from Physics to Technology* (Chichester: John Wiley) p 228
[30] Artacho E, Anglada E, Dieguez O, Gale J D, Garcia A, Junquera J, Martin R M and Ordejon P 2008 *J. Phys.-Condes. Matter* **20** 064208
[31] Fleming S and Rohl A 2005 *Z. Kryst.* **220** 58
[32] Sobon G, Sotor J, Jagiello J, Kozinski R, Zdrojek M, Holdynski M, Paletko P, Boguslawski J, Lipinska L and Abramski K M 2012 *Opt. Express* **20** 19463–73
[33] Xue Y H, Zhu L, Chen H, Qu J and Dai L M 2015 *Carbon* **92** 305–10
[34] Stobinski L, Lesiak B, Malolepszy A, Mazurkiewicz M, Mierzwa B, Zemek J, Jiricek P and Bieloshapka I 2014 *J. Electron Spectrosc. Relat. Phenom.* **195** 145–54
[35] Iwashita N, Park C R, Fujimoto H, Shiraishi M and Inagaki M 2004 *Carbon* **42** 701–14
[36] Ju H, Choi S and Huh S H 2010 *J. Korean Phys. Soc.* **57** 1649–52
[37] Lavanya J, Gomathi N and Neogi S 2014 *Mater. Res. Express* **1** 025604
[38] Beams R, Cancado L G and Novotny L 2015 *Jounal of Physics Condens Matter* **27** 083002 26 pp
[39] Claramunt S, Varea A, Diaz D L, Velazquez M M, Cornet A and Cirera A 2015 *J. Phys. Chem* C **119** 10123–9
[40] Gomez J, Villaro E, Navas A and Recio I *Mater. Res. Express* **4** 105020
[41] Geng D S, Yang S L, Zhang Y, Yang J L, Liu J, Li R Y, Sham T K, Sun X L, Ye S Y and Knights S 2011 *Appl. Surf. Sci.* **257** 9193–8
[42] Ferrari A C and Robertson J 2000 *J. Phys. Rev.* B **61** 14095
[43] Cancado L G, Takai K, Enoki T, Endo M, Kim Y A, Mizusaki H, Jorio A, Coelho L N, Magalhaes-Paniago R and Pimenta M A 2006 *Appl. Phys. Lett.* **88** 163106
[44] Stankovich S, Dikin D A, Piner R D, Kohlhaas K A, Kleinhammes A, Jia Y, Wu Y, Nguyen S T and Ruoff R S 2007 *Carbon* **45** 1558
[45] Rafiee J, Mi X, Gullapalli H, Thomas A V, Yavari F, Shi Y F, Ajayan P M and Koratkar N A 2012 *Nat. Mater.* **11** 217–22
[46] Shih C J, Strano M S and Blankschtein D 2013 *Nat. Mater.* **12** 866–9
[47] Chibowski E and Perea-Carpio R 2002 *Adv. Colloid Interface Sci.* **98** 245–64
[48] Wang S R, Zhang Y, Abidi N and Cabrales L 2009 *Langmuir* **25** 11078–81
[49] Kravets V G, Grigorenko A N, Nair R R, Blake P, Anissimova S, Novoselov K S and Geim A K 2010 *Phys. Rev.* B **81** 155413
[50] Sur U K, Saha A, Datta A, Ankamwar B, Surti F, Roy S D and Roy D 2016 *Bull. Mat. Sci.* **39** 159–65
[51] Ray A K and Hogarth C A 1990 *J. Phys. D-Appl. Phys.* **23** 458–9
[52] Mathkar A, Tozier D, Cox P, Ong P J, Galande C, Balakrishnan K, Reddy A L M and Ajayan P M 2012 *J. Phys. Chem. Lett.* **3** 986–91
[53] Dimitrov V and Sakka S 1996 *J. Appl. Phys.* **79** 1736–40
[54] Wang X F, Chen Y P and Nolte D D 2008 *Opt. Express* **16** 22105–12
[55] Lundie M, Tomic S and Sljivancanin Z 2014 *Phys. Scr.* **T162** 014019

[56] Lundie M, Sljivancanin Z and Tomic S 2015 *J. Mater. Chem.* C **3** 7632–41
[57] Chen P Y, Sodhi J, Qiu Y, Valentin T M, Steinberg R S, Wang Z Y, Hurt R H and Wong I Y 2016 *Adv. Mater.* **28** 3564
[58] Ray A K and Hogarth C A 1984 *Int. J. Electron.* **57** 1–77
[59] Lundie M, Sljivancanin Z and Tomic S *J. Phys.: Conf. Ser.* **526** 012003